geosciences

MDPI

Article

'Silent' Dome Emplacement into a Wet Volcano: Observations from an Effusive Eruption at White Island (Whakaari), New Zealand in Late 2012

Arthur Jolly [1,*], Corentin Caudron [2], Társilo Girona [3], Bruce Christenson [1] and Roberto Carniel [4]

1 GNS Science, Avalon, Lower Hutt 5010, New Zealand; B.Christenson@gns.cri.nz
2 ISTerre, Université Grenoble Alpes, Université Savoie Mont Blanc, 73000 Chambery, France; corentin.caudron@gmail.com
3 Jet Propulsion Laboratory, California Institute of Technology, Pasadena, CA 91109, USA; tarsilo.girona@jpl.nasa.gov
4 Laboratorio di Misure e Trattamento dei Segnali, DPIA, University of Udine, Udine, 33100 Friuli, Italy; carniel1965@gmail.com
* Correspondence: a.jolly@gns.cri.nz

Received: 2 April 2020; Accepted: 9 April 2020; Published: 14 April 2020

Abstract: The 2012–2016 White Island (Whakaari) eruption sequence encompassed six small explosive events that included one steam driven and five explosive phreato-magmatic eruptions. More enigmatic, a dome was observed at the back of the vent and crater lake in November 2012. Its emplacement date could not be easily determined due to persistent steam from the evaporating crater lake and because of the very low levels of discrete volcanic earthquakes associated with its growth. During this period, seismicity also included persistent tremor with dominant frequencies in the 2–5 Hz range. Detailed assessment of the tremor reveals a very slow evolution of the spectral peaks from low to higher frequencies. These gliding spectral lines evolved over a three-month time period beginning in late September 2012 and persisting until early January 2013, when the tremor stabilised. As part of the dome emplacement episode, the crater lake progressively dried, leaving isolated pools which then promoted persistent mud/sulphur eruption activity starting in mid-January 2013. We interpret the emplacement of the dome as a non-explosive process where the hot, mostly degassed, magma intruded slowly through the hydrothermal system in late September 2012 and cooled in a relatively quiet state. The tremor evolution might reflect the slow contraction of subsurface resonant cavities, which increased the pitch of the peak resonant frequency through time. Alternatively, spectral evolution might reflect a 'comb function' due to clockwork beating of the slowly cooling dome, although direct evidence of clockwork beats is not seen in the waveform data. Finally, it might represent frothing of the hydrothermal system ahead of the slowly propagating magma.

Keywords: dome emplacement; hydrothermal system; RSAM; tremor; gliding spectral lines; White Island; phreatic eruptions

1. Introduction

White Island (Whakaari in Te Reo Maori) is a frequently active and hazardous composite cone volcano with most of its relief lying below sea level within the south-eastern Bay of Plenty (Figure 1A). While White Island produces only small eruptions by global standards, the tragic 9 December 2019 event illustrates the possible societal impacts that relate to small eruptions at volcanoes that are frequented by tourists. Such eruptive activity was also present during the 2012–2016 period (Figure 1) which proceeded from the onset of unrest in mid-2011 [1,2], produced several well documented explosive

eruptions [1,3,4] through 2012 and 2013, and culminated in April 2016 with a small phreatomagmatic event [2,5,6].

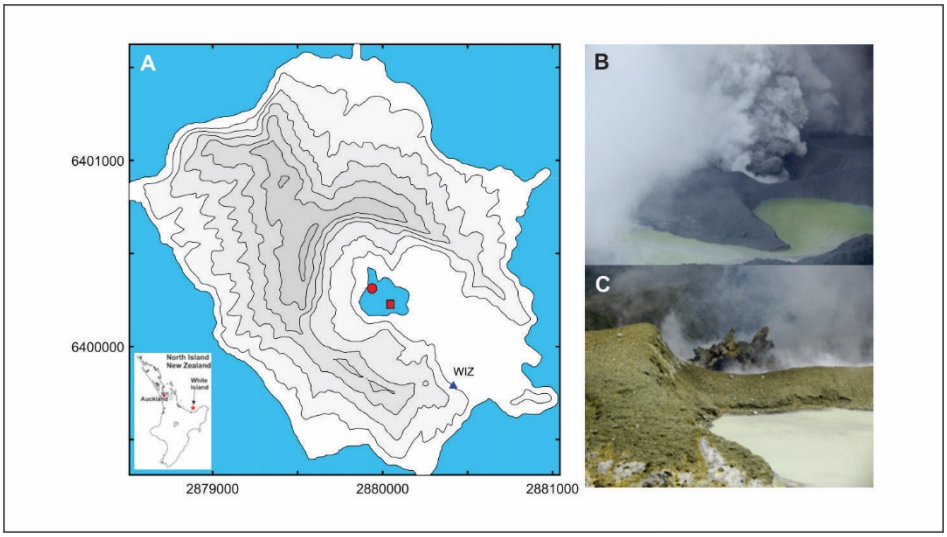

Figure 1. Map of White Island, located in the south-eastern Bay of Plenty (the topographic contour is 40 m). The single seismic station WIZ (blue triangle) and dome eruption vent (red circle) and south east eruption vent (red square) shown in (**A**). Ash venting during the 5 August post eruption ash venting period is shown for 9 August. The dome is shown in (**C**) and was taken 12 December. Note the remainder of the crater lake in the foreground. Photo (**B**) is unattributed courtesy of GeoNet, while (**C**) is by Brad Scott courtesy of GeoNet.

Eruptions at White Island are driven by persistently active magmatic degassing that is evident over the historical record [7]. This degassing requires long-term magmatic injection into shallow portions of the volcanic edifice, which may be accomplished via convective overturn within a conduit [8–10] or persistent injection of small batches of magma [11,12].

A small effusive dome was also emplaced on the back wall margin of the active lake filled eruption vent system, and hence this is an excellent example of magmatic propagation through a 'wet' volcano hydrothermal system. The dome effusion had significant consequences for the evolution of the hydrothermal system, promoting the drying of the lake, and a switch to persistent and well documented mud/sulphur eruption activity [13–16]. Dome forming eruptive activity is a frequent occurrence in volcanic systems with viscous magmas and have drawn significant scientific interest due to their persistent medium- to long-term hazards. These hazards are greatest when the domes are perched at elevation on unstable slopes of a volcanic edifice such as at volcanoes like Soufriere Hills, Montserrat [17]; Redoubt, Alaska [18]; or Merapi, Indonesia [19]. Domes may also form within positions of lower relief (e.g., Mt. St. Helens [20–22]), and in such cases, the eruptions can be emplaced through well-developed hydrothermal systems.

The hydrothermal system at White Island results from the interaction between magmatic heat and juvenile fluids with water from meteoric and oceanic sources that percolates into the crust [16]. Heat and fluids from the magma drive convective circulation that establish fluid phase transitions below the surface and a hydrostatically controlled phase equilibrium with its enclosing hydrothermal brine. In particular, at the magma-hydrothermal system interface, a single-phase gas enveloped by a two-phase fluid composed of liquid and gas bubbles dominates, whereas a single-phase liquid will eventuate at shallow levels and within the crater lake. These conditions are generally stable but can evolve in different ways depending on the position of magma within the system and externally modulating effects like rainfall (Figure 2).

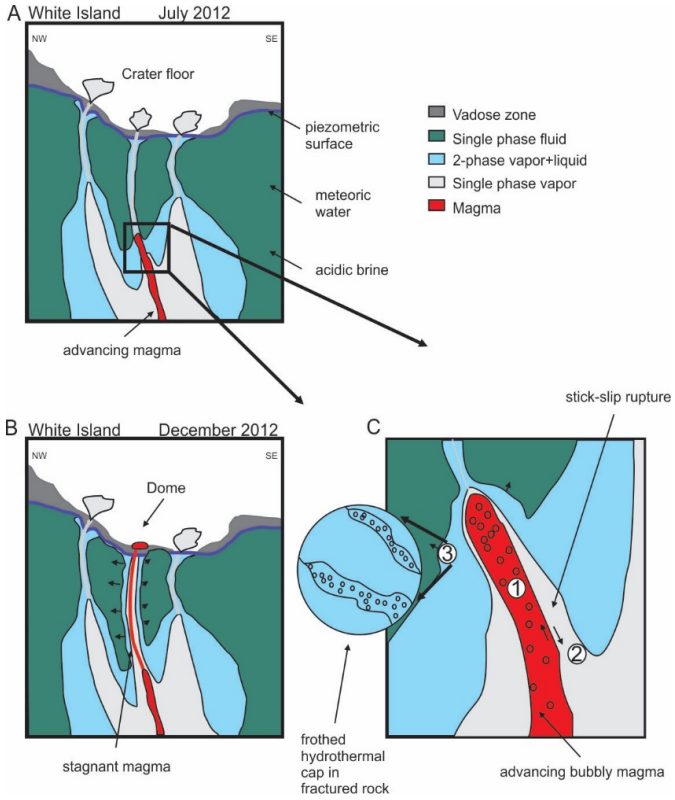

Figure 2. Schematic cross section depicting (**A**) the pre- and (**B**) post-extrusion scenarios for the dome. Acidic brine fluids underlie meteoric water/condensate lenses (both depicted green) and encapsulate the magmatic/fumarolic vent system (blue and grey). Magma ascends along the main conduit (designated by the red line in (**B**), preceded by increased heat and gas flow which evaporates the two-phase vapour-liquid region to single-phase vapor along its way (grey). Three possible resonant systems are portrayed in the inset diagram (**C**). The bubble filled cavity (1). A clockwork stick-slip rupture mechanism (2), or the frothed expanding boiling front (3 and its inset) may produce harmonic signals discussed. The arrows in B show the expanded two-phase system that results from the propagating magma injection. See text.

From a seismological perspective, the shallow hydrothermal system may produce the full range of seismic observations seen at White Island and its global analogues like Kawah Ijen volcano, Indonesia [4,23]. Examples include discrete long-period (LP) [24], volcano-tectonic (VT) [2,25], very long period (VLP) seismicity [2], and persistent volcanic tremor [1]. Tremor is an important feature of volcanic seismicity [26]. It is characterised by a continuous, banded, or spasmodic signal, which is detectable only when exceeding the background seismic energy level [26]. Several data reduction methods [27] have been proposed to characterize its short- and long-term time evolution, that can lead to the identification of significant transitions between volcanic processes [28], sometimes triggered by external or internal events such as tectonic or volcano-tectonic (VT) seismic events [29]. Volcanic tremor can also occur precursory to an eruption [30–33]. However, the origins of tremor may vary at different volcanoes, and are often poorly understood; moreover, many different seismic sources can act at the same time and combine to produce the signal of interest [27].

Harmonic tremor, consisting of a fundamental frequency and evenly spaced overtones, is a common occurrence at volcanic systems worldwide [34,35], and is important both to determine possible source processes and as a monitoring tool. Changing spectral patterns in harmonic tremor (e.g., migration of the spectral lines, i.e., so-called gliding) is increasingly recognised at volcanoes [36–38] as an important short-term precursor that may occur several minutes prior to explosive activity.

Systematic evolution of spectra over longer time periods are less common; however, an assessment of such slowly evolving systems may also be important from a process and hazard standpoint [39].

It is surmised that movement of magma below or within a hydrothermal system should produce significant changes in seismic observations [40–42] (Figure 2). Hence, the extrusion of magma through a well-established hydrothermal system and onto the surface provides an excellent opportunity to re-examine remote monitoring data for hazards implications. The dome forming eruption at White Island is interesting in this context because its discovery was truly enigmatic. It was first documented by GeoNet on 11 December 2012 but was observed by White Island tour operators possibly a fortnight earlier (Volcanic Alert Bulletin WI-2012/16; https://www.geonet.org.nz). Surprisingly, its emplacement occurred without dramatic seismicity revealed on the permanent White Island seismic station (Figure 1A). Likewise, an evaluation of the White Island web camera system did not reveal the appearance of the small dome, mostly due to persistent obscuring steam plumes for the period from the initial onset of eruption activity on 5 August 2012 [1]. It also appeared to have been quite effusive, based on the smooth lumpy texture of the surface (Figure 1C). The dome, with an extent of 20–30 m in diameter and a height of 10–15 m, has a volume on the order of $1–7 \times 10^3$ m^3. Below, we retrospectively document the pre-eruption seismicity from the onset of eruptive activity from August to the observation of the dome in December 2012.

2. Seismic Data and Results

White Island seismic monitoring was composed of a single broadband seismic sensor at site WIZ (Figure 1A), which is comprised of a Guralp 3ESP seismometer and a Quanterra Q330 digitiser, sampling at 100 Hz and telemetering data in real time to the GeoNet data center. The archived seismic data were processed in two ways: (1) calculation of the real-time seismic amplitude measurement value (RSAM) by taking the time-series data from the vertical component sensor, correcting it to velocity, and computing the root mean square (RMS) amplitude within one minute long, non-overlapping windows (Figure 3A); and (2) computing the spectra via the fast-Fourier transform (FFT) for each one-minute window (Figure 3B). For the latter, we visualised the data by picking the peak amplitude from the spectra and monitoring that over the period of interest (before the first eruption to the end of the dome forming phase).

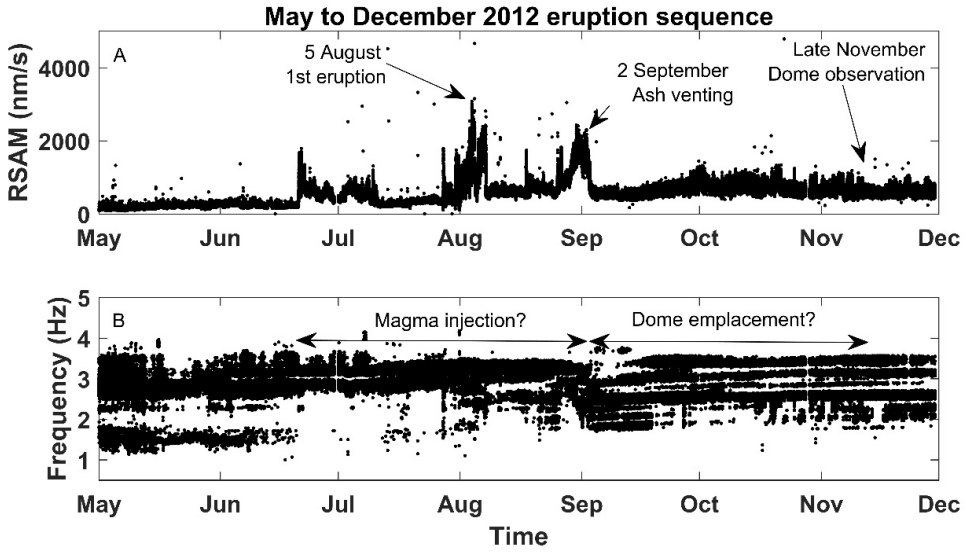

Figure 3. Real-time seismic amplitude measure (RSAM) computed from one-minute moving windows (**A**) and the maximum spectral peak amplitude (**B**) from Fast Fourier Transform of the same one-minute window. The 6 August 6 eruption and 2 September ash venting episode and the dome emplacement are marked (**A**) and the inferred injection of magma into the deeper hydrothermal system and emplacement of the dome are shown in (**B**).

The one-minute RSAM observations (Figure 3A) show the first eruption on 5 August 2012 (RSAM~2800 nm/s), as well as a persistent high amplitude signal in early September (~2100 nm/s), followed by sustained moderate level tremor (500–1000 nm/s) through the time of the dome observation in late November 2012. The spectral analysis (Figure 3B) shows that the peak frequency of tremor is generally focused within the ~1.0–4.0 Hz band, with specific and persistent peaks and notable evolutionary patterns. We note with particular interest the spectral changes associated with high amplitude tremor periods, including (1) a shift from broader spectrum tremor to 2.5–3.5 Hz in mid-June 2012; (2) the onset of a migration of the spectral peaks (termed gliding spectral lines in the literature [36]) in mid-July; (3) the onset of broader spectra tremor with slowly gliding spectral lines in early September; and (4) establishment of stable (non-gliding) persistent spectral peaks in late December (see red dots in Figure 4). These spectral changes of tremor are linked in time to specific aspects of volcanic activity, including: (A) Rapid volcanic lake fluctuations of about 4 m and minor geysering (observed in June/July); (B) the onset of the first strong eruption on 5 August; (C) persistent ash venting in early September; and (D) the first observation of the dome in late November.

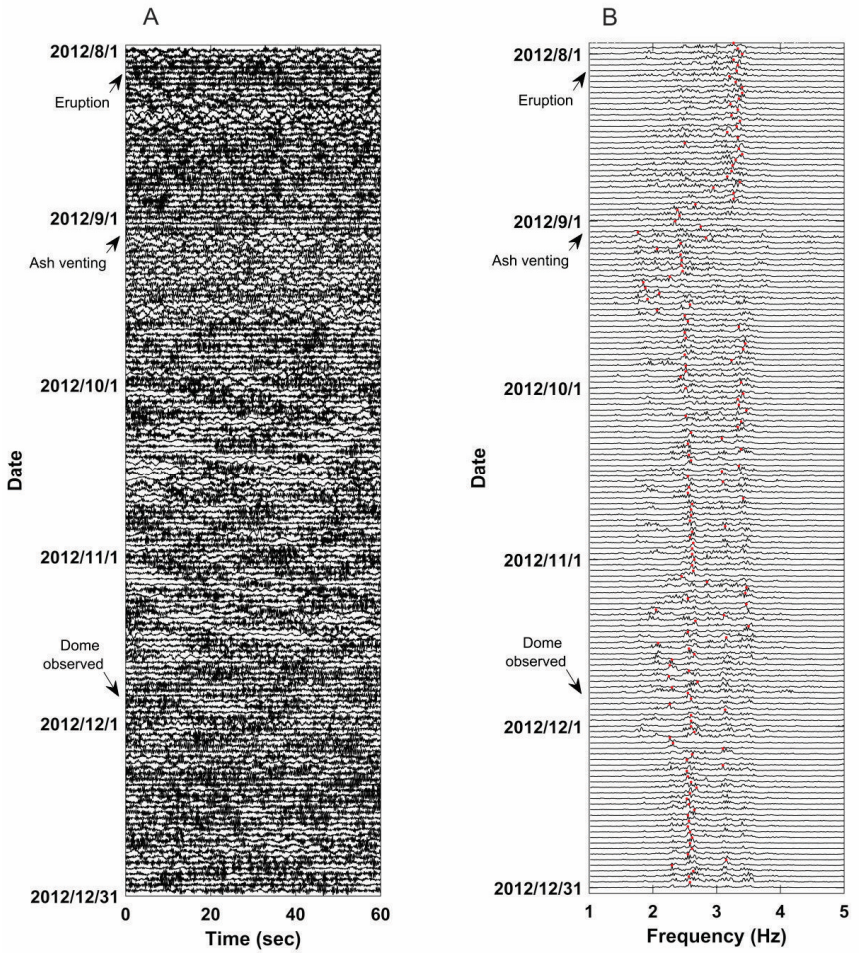

Figure 4. Example waveforms (**A**) and spectra (**B**) for a subset of the seven-month period of interest. The examples are extracted from the continuous seismic data and include one minute from the start of each Julian day (UT HH:MM 00:00 to 00:01). The initial eruption occurred on 5 August 2012 at NZST 04:55, and the waveforms are not shown. Note the change in peak frequency around the time of the secondary ashing on 2 September 2012 NZST. Also note the slow migration of peak frequencies until the observation of the dome (note red marks for peak spectral frequency). The crater was largely obscured by steam from the period of ashing to the observation of the dome.

To aid in interpreting the seismic observations, example waveforms (Figure 4A) and spectra (Figure 4B) are plotted from the first minute of each day for the period 1 July to 31 December 2012 (Figures 3 and 4 are presented in UTC). Although we realize that this procedure potentially produces an aliasing effect, the individual sample waveforms and spectra match closely a denser spectral analysis and confirm the observations in Figure 3. Hence, we regard the observations in Figures 3 and 4 as robust, illustrating both the longer-term features of the tremor and the slowly evolving migration from lower to higher spectral frequencies.

Specific spectral peaks become well established in late August 2012, which then perceptibly migrate towards higher frequencies over a three-month period. On ~ 29 August 2012, the specific peaks of interest are at 2.1 Hz (Figure 4B). These peaks shift to a stable frequency of 2.3 Hz by 30 November 2012 (Figure 4B), about the same period that the dome must have been emplaced based on the tremor and the first observation of the dome. A subsidiary peak is also observed, which weakly emerges at ~2.9 Hz after the ashing episode and persists after the first dome observation at a modestly higher frequency of ~ 3.2 Hz. There are also stationary spectral peaks observed at other specific frequencies (Figures 3 and 4B) as part of a possible harmonic pattern which began in early September and evolved until the dome was observed.

To assess possible harmonic patterns, we computed spectrograms using two-minute-long windows. Each time window is detrended with a mean and a linear function before tapering using a Hanning window (10% on each side). The frequency resolution is 0.0083 Hz. For each column of the spectrogram the resulting FFT amplitudes are color-coded and shown in Figure 5. After smoothing the results with a median of five days, we picked the central frequencies of continuous spectral lines: 1.4, 1.6, 1.8, 2.0, 2.2, 2.3, 2.7, 2.9, 3.2, 3.5, 4.9 Hz. We note that 2.2 Hz and 2.3 Hz seem to merge in September.

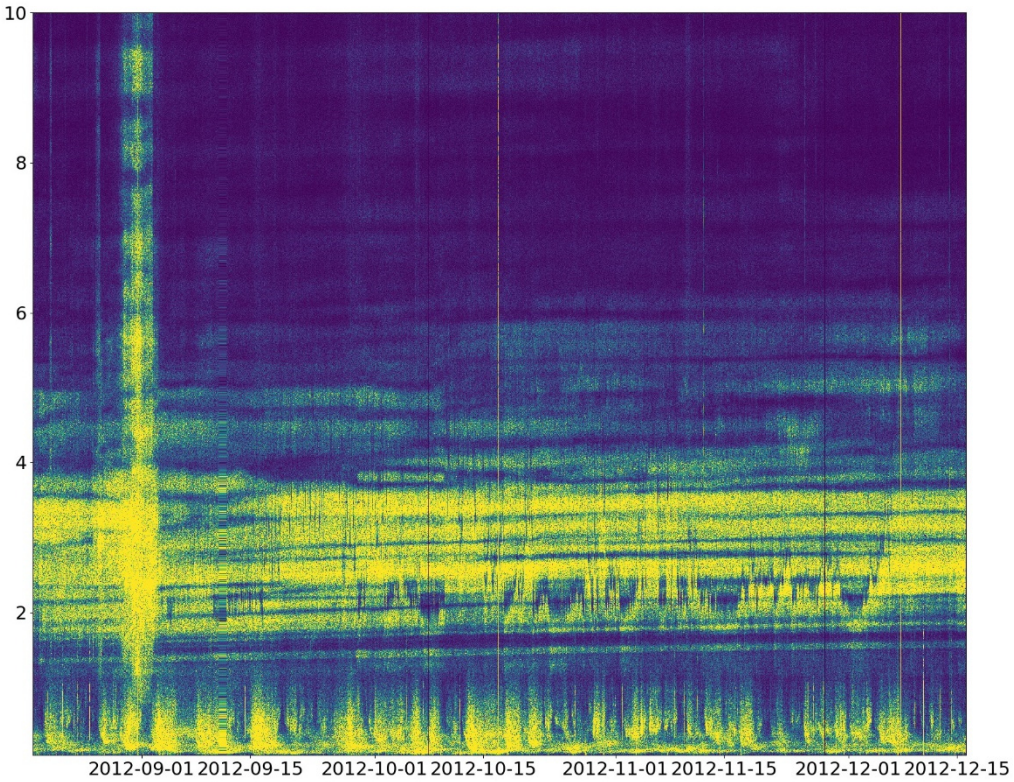

Figure 5. Spectrogram computed using two-minute-long windows after removing the mean, the trend and applying a cosine taper in each window. Yellow colours correspond to high amplitudes, whereas blue colours correspond to low amplitudes.

We then assess if the data were consistent with a harmonic tremor source. In fact, although peaks often appear to be equally spaced in frequency, the dominant frequency is rarely seen. We therefore developed an algorithm to automatically compute this possibly buried dominant frequency.

For each column of the spectrogram (i.e., 2 min), the algorithm determines all the peaks by looking for local maxima in the column. An histogram of these peaks is then built over a wider time window (e.g., 4 h or 12 h) by counting for each frequency how many times a peak is detected. Finally, we search for our dominant frequency in the 0.3–1.3 Hz range, and cumulate histogram values not only for that candidate dominant frequency but also for its potential harmonics. The cumulated value is then normalized (i.e. divided by the number of harmonics) because lower frequencies may yield higher numbers of harmonics and higher cumulated values.

For each column, we determine the potential dominant frequency, and we superimpose it, together with all its harmonics, on the spectrogram to assess its coherency with time. The results (Figure 6 for time windows of 4 h, and in Figure 7 for time windows of 12 h) are consistent with a harmonic oscillation over a narrow frequency band, hence confirming that the tremor could originate from a harmonic process. We must acknowledge that the observation is based on the sole single station observation and hence may include other influences such as path and structural effects in this complex volcanic edifice.

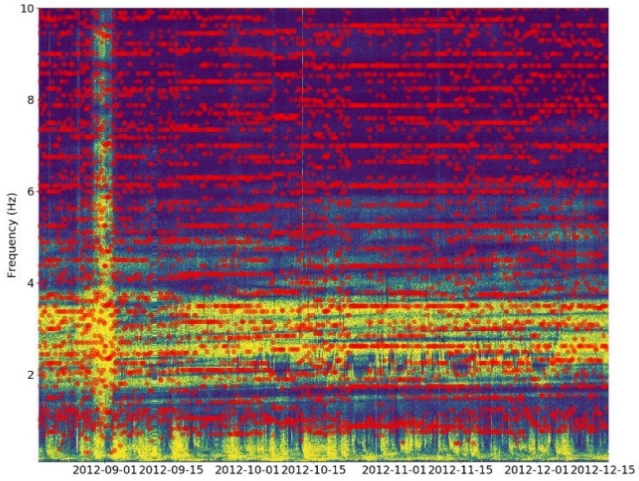

Figure 6. Same as Figure 5, but with potential dominant frequency and corresponding harmonics overlaid (red dots in 4-hr time windows).

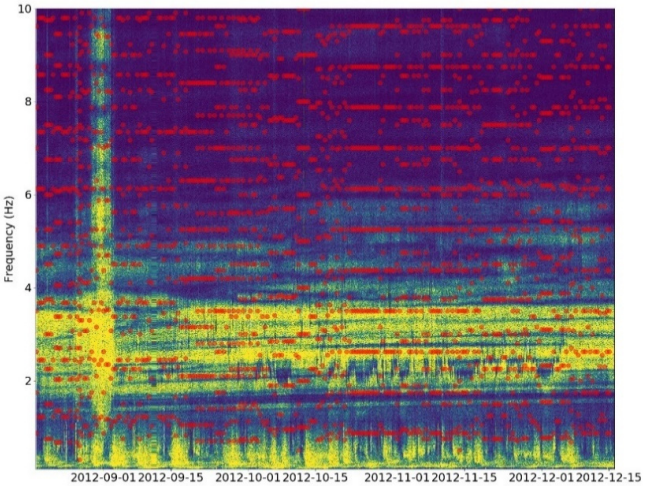

Figure 7. Same as Figure 6, but with potential dominant frequency and corresponding harmonics overlaid (12-hr time windows).

3. Discussion

Whilst the migration in spectral peaks is very small compared to other well-known examples like Soufriere Hills [36] and Redoubt [38], the spectral gliding observed for White Island occurs over a much longer time period of ~3–4 months. This timescale is more comparable to the one observed at Villarrica volcano [43], although in that case the frequency changes were more abrupt. In all of these cases, the spectral changes can be linked to eruptive activity at the volcano. The gliding frequencies at White Island are unusual in two respects. First, they persisted over several months, starting with the onset of low-level ash eruptions in early September 2012, and the observation of a dome over 2.5 months later in late November. Second, while the gliding spectral lines observed prior to large eruptive events (e.g., Soufriere Hills [36]; Redoubt [38]) seem to have persistent monotonically increasing frequencies (concave upward trending spectral peaks) for fundamental frequencies and overtones, the observations here include increasing spectral peak-lines with a reduced rate of change over time (i.e., a concave downward increase in frequency). This observation might suggest a different mechanism for the two processes (Figures 3B and 5).

Harmonic features in seismic data are often regarded as part of three potential processes, including fluid-elastic [39,40,44–54], frictional-induced [38,41], and permeable flow-controlled resonance [42,46]. In the first source process (see Figure 2C label (1)), fluid-elastic resonance involves the vibrations of cavities as a result of the motion of fluids in response to short-term perturbations (e.g., possibly the superposition of hybrid earthquakes thought to occur as magma proceeds through the glass transition at shallow depth [55]. In such a case, the different modes of vibration vary with the impedance contrast (i.e., with the properties of the fluid filling the cavity) and geometry [35,56–58]. In the second source process (Figure 2C label (2)), a frictional mechanism involves the generation of harmonic tremor by the superposition of highly regular repetition of mostly identical stick-slip earthquakes [41]. In such a case, the dominant frequencies vary with the elastic properties of the medium, stressing rates, and geometry, whereas overtones are the result of a Dirac comb effect. In the third source process (see Figure 2C label (3)), a permeable flow-controlled mechanism involves the spontaneous vibration of cavities while gas escapes toward the surface and is the result of the transient porous flow of magmatic/hydrothermal gases through the permeable medium that caps the cavity. In such a case, the pressure inside the cavity is governed by the equation of a non-linear oscillator, which reduces to a linear first-order harmonic oscillator for highly-fractured and thin ($\lesssim$100 m) caps [42]; hence, the specific frequencies depend on the permeability and porosity of the cap, gas properties, supply, and geometry of the cavity. In particular, a harmonic tremor may emerge through a Dirac comb effect when gas feeds the cavity regularly (e.g., through bubble clouds or foam collapse, [59–61]. Alternatively, a harmonic tremor may arise as a non-linear effect [46] or for thick ($\gtrsim$ 100 m) caps as result of the high-order terms controlling the pressure oscillations of the cavities [42].

At White Island, the observation of the dome in late November 2012 and the lack of strong seismicity associated with its appearance is enigmatic and can provide some constraints regarding the governing tremor mechanism. Persistent steam obscured the back of the crater lake and this might imply that the dome had been emplaced much earlier, possibly around the 2 September ash venting period shown in Figure 4. If this did mark the dome emplacement, then the slow cooling of the dome and conduit may have contributed to the spectral gliding within the tremor. For example, the slow progressive cooling and degassing might provide both the required seismic trigger mechanism and the higher impedance contrast cavity to produce harmonic tremor through fluid-elastic resonance. If a magmatic root remained beneath the dome, such a feature could hold exsolved gases within a bubble-rich root structure; Neuberg and O'Gorman [58] have shown how such a conduit could produce resonant tremor. If this conduit became progressively further degassed or if progressive top down solidification occurred, this could produce a smaller conduit with time. The slowly evolving changes in tremor might then reflect variations of the resonant root structure.

As an alternative, the slowly evolving spectral features could be regarded as a feature of the emplacement process if the dome were emplaced shortly before its observation in late November.

The 2–5 Hz tremor source process at White Island, thought to be dominantly within the hydrothermal system, is a long-term feature of the shallow volcanic system [1]. In this case, the modulation of the shallow seismicity might reflect a longer-term intrusion process at depth. If the sub-surface magma began its interaction with the shallow hydrothermal system about 2.5 months before the dome's observation, then the ascent rate of intrusion would have been very slow. We regard this alternative as less likely due to the apparent fluidity of the dome features, however it might be relevant to the spectral observations occurring prior to the 5 August explosive eruption (see Figure 3B).

Regarding the second source process (Figure 2), in order to produce clear overtones in the spectrogram, the repetition interval of seismic events must be very precise. However, we do not observe clear discrete earthquakes in the sequence (Figure 4A), so the application of a repeating clockwork pattern, and thus frictional-induced resonance, is not easy to invoke for White Island in this period. In any case, it might be possible for interactions of hydrothermal system fluids with the conduit walls to act as a source of persistent micro-seismicity. Whilst the occurrence of a regular clockwork pattern is not apparent in the waveform data (Figure 4A), it could still be part of the underlying tremor excitation process. This process might also be only weakly periodic but still interact with a nearby resonant cavity [62]. If, on the other hand, the dome was extruded immediately prior to its first observation in November, it is plausible that the tremor observed over the period September to November could be the result of interaction between the ascending magma column and the hydrothermal system through which it is moving. In Figure 2C labeled (3), we illustrate this process with the front of the ascending plug intruding into the overlying two-phase vapor–liquid region extant at the time. This process could explain the earlier June to September spectral features. Temperature gradients above the ascending magma are very high, ranging from an assumed sub-liquidus intrusion temperature of ~ 900 °C to the temperature of the vapour–liquid saturation curve. The overlying conduit, assumed to be a porous fractured medium, is two-phase over its entire length to the surface (see Figure 2C). This conduit could deliver non-condensable gas to an overlying compressible "gas pocket" created beneath a partial mineralogic seal. Such a seal system is argued to be present based on C/S ratios of vent emissions at the time [16].

Gas pockets trapped beneath permeable media or embedded in cracks within the dome may lead to spontaneous vibrations while gas escapes toward the surface [42] but also through thermal instabilities [54]. In these resonant gas pockets, gliding spectral behaviour results from changing lengths of the cavity, with shorter lengths generating progressively higher frequencies over the spectral range of 0.1 Hz to 15 Hz. It is possible that this could result from shortening of the conduit cavity during magma ascent, although this process cannot be definitively confirmed by the existing data. Whereas spectral gliding would be complete when the magma reaches the surface, a tremor would be ongoing during cooling and the ongoing interaction between the plug/dome with the hydrothermal system, as portrayed in Figure 2C.

We regard propagation and emplacement of the dome in early September as more likely due to the strong tremor and the relatively abrupt change of the spectral patterns (Figure 3). If so, then the perturbation of the hydrothermal system led to high levels of gas and steam discharge, which obscured the dome, and caused the observed spectral gliding. It also may have promoted the slow evaporation of the crater lake system, which was a central feature of the White Island crater vent for more than 10 years before the 2012–2016 eruption episode. Regardless of the timing and mechanism of emplacement and stabilisation, it is remarkable for a dome to be emplaced into an active wet hydrothermal system with such subtle changes of the observed tremor patterns.

4. Conclusions

We describe the visual and seismic observations related to the onset of eruptive activity at White Island, New Zealand, for the period June to December 2012. The period included an explosive eruption, ash venting, and a dome emplacement episode through a 'wet' volcano hydrothermal system. The period was marked by persistent elevated tremor amplitudes and slowly evolving gliding spectral

lines. At the same time, the crater lake system progressively evaporated, which encompassed the full crater floor in June 2012 and progressed to isolated pools by the end of December 2012. Interestingly, this progressive lake loss promoted the next phase of mud/sulphur eruptions which began in mid-January 2013 [13–16] through the pre-existent Southeast vent system (Figure 2).

We regard the injection of magma into the shallow hydrothermal system as the key driver of the lake loss and shifts in tremor patterns in mid to late 2012. We interpret that the magmatic intrusion into the hydrothermal system began in early September and promoted the range of seismic observations documented here. Future work will be needed to examine the plausibility of the models outlined here with a rigorous analytical and numerical approach.

As a final note, the 9 December 2019 White Island eruption occurred within the timeframe of the development of this research and post-eruption unrest associated with that eruption is ongoing at the time of writing. Hence, this work does not include new insights from this most recent eruptive activity. At the conclusion of the present unrest period, a detailed retrospective assessment of the progression of unrest will be critical to determine similarities and differences for the two time periods. It is hoped that such an analysis will lead to ever-improving outcomes at difficult to monitor volcanoes like White Island. The present work illustrates how persistent shallow magma and well-developed hydrothermal systems may produce observations that may fit many possible conceptual models and produce challenging monitoring conditions. It is a central goal of the volcano science community to document such events and hence to improve monitoring outcomes for similar volcanic systems both in New Zealand and around the globe. This work will help to assess the viability of the various models within the context of the limited available data.

Author Contributions: Conceptualization, A.J., C.C., T.G.; B.C., and R.C.; Data curation, A.J.; Formal analysis, A.J., C.C., T.G., and R.C.; Investigation, A.J., C.C., T.G., B.C., and R.C.; Methodology, A.J., C.C., T.G. and R.C.; Visualization, A.J., C.C., T.G., B.C., and R.C.; Writing—original draft, A.J., C.C., T.G., B.C., and R.C.; Writing—review and editing, A.J., C.C., T.G., B.C., and R.C. All authors have read and agreed to the published version of the manuscript.

Funding: This research received no external funding.

Acknowledgments: This work used GeoNet seismic data which is freely available. All of the authors contributed toward manuscript and figure production as well as the data analysis and interpretation. Photos used in this study are from the GNS volcano database (VolcDB) and reflects the effort of the GeoNet team. A. Jolly and B. Christenson are supported by the Ministry of Business, Innovation and Employment (MBIE) Strategic Science Investment Fund (SSIF). T. Girona is supported by an appointment to the NASA Postdoctoral Program at the Jet Propulsion Laboratory, California Institute of Technology, administered by Universities Space Research Association under contract with the National Aeronautics and Space Administration. Chris Van Houtte and Tony Hurst reviewed an earlier version of the manuscript. We thank Alicia Hotovec-Ellis, William Chadwick, and a third reviewer for their useful comments which improved the manuscript.

Conflicts of Interest: The authors declare no conflict of interest.

References

1. Chardot, L.; Jolly, A.D.; Kennedy, B.; Fournier, N.; Sherburn, S. Using volcanic tremor for eruption forecasting at White Island volcano (Whakaari), New Zealand. *J. Volcanol. Geotherm. Res.* **2015**, *302*, 11–23. [CrossRef]
2. Jolly, A.D.; Lokmer, I.; Thun, J.; Salichon, J.; Fry, B.; Chardot, L. Insights into fluid transport mechanisms at White Island from analysis of coupled very long-period (VLP), long-period (LP) and high-frequency (HF) earthquakes. *J. Volcanol. Geotherm. Res.* **2017**, *343*, 75–94. [CrossRef]
3. Jolly, A.; Lokmer, I.; Christenson, B.; Thun, J. Relating gas ascent to eruption triggering for the April 27, 2016, White Island (Whakaari), New Zealand eruption sequence. *Earth Planets Space* **2018**, *70*, 177. [CrossRef]
4. Caudron, C.; Taisne, B.; Neuberg, J.; Jolly, A.D.; Christenson, B.W.; Lecocq, T.; Suparjanh; Syahbana, D.; Suantika, G. Anatomy of phreatic eruptions. *Earth Planets Space* **2018**, *70*, 168. [CrossRef]
5. Walsh, B.; Procter, J.; Lokmer, I.; Thun, J.; Hurst, A.W.; Christenson, B.W.; Jolly, A.D. Geophysical examination of the 27 April 2016 Whakaari/White Island, New Zealand, eruption and its implications for vent physiognomies and eruptive dynamics. *Earth Planets Space* **2019**, *71*. [CrossRef]

6. Kilgour, G.N.; Gates, S.; Kennedy, B.M.; Farquhar, A.; McSporran, A.; Asher, C. Phreatic eruption dynamics derived from deposit analysis: A case study from a small phreatic eruption from Whakaari/White Island, New Zealand. *Earth Planets Space* **2019**. [CrossRef]
7. Werner, C.A.; Hurst, A.W.; Scott, B.J.; Sherburn, S.; Christenson, B.W.; Britten, K.; Cole-Baker, J.; Mullan, B. Variability of passive gas emissions, seismicity, and deformation during crater lake growth at White Island Volcano, New Zealand, 2002–2006. *J. Geophys. Res.* **2008**, *113*, 15. [CrossRef]
8. Kazahaya, K.; Shinohara, H.; Saito, G. Excessive degassing of Izu-Oshima volcano: Magma convection in a conduit. *Bull. Volcanol.* **1994**, *56*, 207–216. [CrossRef]
9. Stevenson, D.S.; Blake, S. Modelling the dynamics and thermodynamics of volcanic degassing. *Bull. Volcanol.* **1998**, *60*, 307–317. [CrossRef]
10. Harris, A.; Carniel, R.; Jones, J. Identification of variable convective regimes at Erta Ale Lava Lake. *J. Volcanol. Geotherm. Res.* **2005**, *142*, 207–223. [CrossRef]
11. Cole, J.W.; Thordarson, T.; Burt, R.M. Magma Origin and Evolution of White Island (Whakaari) Volcano, Bay of Plenty, New Zealand. *J. Pet.* **2005**, *41*, 867–895. [CrossRef]
12. Girona, T.; Costa, F.; Schubert, G. Degassing during quiescence as a trigger of magma ascent and volcanic eruptions. *Sci. Rep.* **2015**, *5*, 18212. [CrossRef] [PubMed]
13. Jolly, A.D.; Kennedy, B.; Edwards, M.; Jousset, P.; Scheu, B. Infrasound tremor from bubble burst eruptions in the viscous shallow crater lake of White Island, New Zealand, and its implications for interpreting volcanic source processes. *J. Volcanol. Geotherm. Res.* **2016**, *327*, 585–603. [CrossRef]
14. Edwards, M.J.; Kennedy, B.M.; Jolly, A.D.; Scheu, B.; Jousset, P. Evolution of a small hydrothermal eruption episode through a mud pool of varying depth and rheology, White Island, NZ. *Bull. Volcanol.* **2017**, *79*. [CrossRef]
15. Schmid, D.; Scheu, B.; Wadsworth, F.B.; Kennedy, B.M.; Jolly, A.D.; Dingwell, D.B. A viscous-to-brittle transition in eruptions through clay suspensions. *Geophys. Res. Letts.* **2017**, *44*, 4806–4813. [CrossRef]
16. Christenson, B.W.; White, S.; Britten, K.; Scott, B.J. Hydrological evolution and chemical structure of a hyper-acidic spring-lake system on Whakaari/White Island. New Zealand. *J. Volcanol. Geotherm. Res.* **2017**, *346*, 180–211. [CrossRef]
17. Watts, R.B.; Herd, R.A.; Sparks, R.S.J.; Young, S.R. Growth Patterns and Emplacement of Andesitic Lava Dome at Soufriere, Hills, Volcano, Montserrat. In *The Eruption of Soufriere Hills Volcano, Montserrat, from 1995 to 1999*; Druitt, T.H., Kokelaar, B.P., Eds.; The Geological Society of London: London, UK, 2002; Volume 21.
18. Bull, K.F.; Anderson, S.W.; Diefenbach, A.K.; Wessels, R.L.; Henton, S.M. Emplacement of the final lava dome of the 2009 eruption of Redoubt Volcano, Alaska. *J. Volcanol. Geotherm. Res.* **2013**, *259*, 334–348. [CrossRef]
19. Hammer, J.E.; Cashman, K.V.; Voight, B. Magmatic processes revealed by textural and compositional trends in Merapi dome lavas. *J. Volcanol. Geotherm. Res.* **2000**, *100*, 165–192. [CrossRef]
20. Moore, J.G.; Lipman, P.W.; Swanson, D.; Alpha, T.R. Growth of lava domes in the crater, June 1980-January 1981. In *The 1980 Eruptions of Mt St. Helens*; Lipman, P.W., Mullineaux, D.R., Eds.; Geological Survey research Professor Paper; USGS: Washington, DC, USA, 1981; Volume 1250.
21. Swanson, D.A.; Dzurisin, D.; Holcomb, R.T.; Iwatsubo, E.Y.; Chadwick, W.W.; Casadevall, T.J.; Ewert, J.W.; Heliker, C.C. Growth of the lava dome at Mount St. Helens, Washington, 1981–1983. In *The Emplacement of Silicic Domes and Lava Flows*; Fink, J., Ed.; The Geological Society of America Special Paper; Geological Society of America: Boulder, CO, USA, 1987; Volume 212, pp. 1–16.
22. Vallance, J.W.; Schneider, D.J.; Schilling, S.P. Growth of the 2004–2006 Lava-Dome Complex at Mount St. Helens, Washington. *USGS Prof. Pap.* **2008**, *1750*, 169–208.
23. Caudron, C.; Syahbana, D.K.; Lecocq, T.; Van Hinsberg, V.; McCausland, W.; Triantafyllou, A.; Camelbeeck, T.; Bernard, A. Kawah Ijen volcanic activity: A review. *Bull. Volcanol.* **2015**, *77*, 16. [CrossRef]
24. Sherburn, S.; Scott, B.J.; Nishi, Y.; Sugihara, M. Seismicity at White Island volcano, New Zealand: A revised classification and inferences about source mechanism. *J. Volcanol. Geotherm. Res.* **1998**, *83*, 287–312. [CrossRef]
25. Carniel, R. Comments on the paper "Automatic detection and discrimination of volcanic tremors and tectonic earthquakes: An application to Ambrym volcano, Vanuatu" by Daniel Rouland; Denis Legrand; Mikhail Zhizhin; Sylvie Vergniolle. *J. Volcanol. Geotherm. Res.* **2010**, *194*, 61–62. [CrossRef]
26. Konstantinou, K.; Schlindwein, V. Nature, wavefield properties and source mechanism of volcanic tremor: A review. *J. Volcanol. Geotherm. Res.* **2003**, *119*, 161–187. [CrossRef]

27. Carniel, R. Characterization of volcanic regimes and identification of significant transitions using geophysical data: A review. *Bull. Volcanol.* **2014**, *76*, 848. [CrossRef]
28. Tárraga, M.; Martí, J.; Abella, R.; Carniel, R.; López, C. Volcanic tremors: Good indicators of change in plumbing systems during volcanic eruptions. *J. Volcanol. Geotherm. Res.* **2014**, *273*, 33–40. [CrossRef]
29. Carniel, R.; Tárraga, M. Can tectonic events change volcanic tremor at Stromboli? *Geophys. Res. Lett.* **2006**, *33*, 4–6. [CrossRef]
30. Chouet, B.A.; Matoza, R.S. A multi-decadal view of seismic methods for detecting precursors of magma movement and eruption. *J. Volcanol. Geotherm. Res.* **2013**, *252*, 108–175. [CrossRef]
31. Girona, T.; Huber, C.; Caudron, C. Sensitivity to lunar cycles prior to the 2018 eruption of Ruapehu volcano. *Sci. Rep.* **2018**, *8*, 1476. [CrossRef]
32. Ortiz, R.; García, A.; Marrero, J.M.; De la Cruz-Reyna, S.; Carniel, R.; Vila, J. Volcanic and volcano-tectonic activity forecasting: A review on seismic approaches. *Ann. Geophys.* **2019**, *62*. [CrossRef]
33. Caudron, C.; Girona, T.; Taisne, B.; Suparjan; Gunawan, H.; Kasbani; Kristianto. Change in seismic attenuation as a long-term precursor of gas-driven eruptions. *Geology* **2019**, *47*, 632–636. [CrossRef]
34. Sherburn, S.; Scott, B.J.; Hurst, A.W. Volcanic tremor and activity at White Island, New Zealand, July–September 1991. *N. Z. J. Geol. Geophys.* **1996**, *39*, 329–332. [CrossRef]
35. Neuberg, J. Characteristics and causes of shallow seismicity in andesite volcanoes. *Philos. Trans. R. Soc. Lond. A* **2000**, *358*, 1533–1546. [CrossRef]
36. Powell, T.W.; Neuberg, J. Time dependent features in tremor spectra. *J. Volcanol. Geotherm. Res.* **2003**, *128*, 177–185. [CrossRef]
37. Lesage, P.; Mora, M.M.; Alvarado, G.E.; Pacheco, J.; Métaxian, J. Complex behavior and source model of the tremor at Arenal volcano, Costa Rica. *J. Volcanol. Geotherm. Res.* **2006**, *157*, 49–59. [CrossRef]
38. Hotovec, A.J.; Prejean, S.G.; Vidale, J.E.; Gomberg, J. Strongly gliding harmonic tremor during the 2009 eruption of Redoubt Volcano. *J. Volcanol. Geotherm. Res.* **2013**, *259*, 89–99. [CrossRef]
39. Ripepe, M.; Gordeev, E. Gas bubble dynamics model for shallow volcanic tremor at Stromboli. *J. Geophys. Res.* **1999**, *104*, 10639–10654. [CrossRef]
40. Julian, B.R. Volcanic tremor: Nonlinear excitation by fluid flow. *J. Geophys. Res.* **1994**, *99*, 11859–11877. [CrossRef]
41. Dmitrieva, K.; Hotovec-Ellis, A.J.; Prejean, S.; Dunham, E.M. Frictional-faulting model for harmonic tremor before Redoubt Volcano eruptions. *Nat. Geosci.* **2013**, *6*, 652–656. [CrossRef]
42. Girona, T.; Caudron, C.; Huber, C. Origin of shallow volcanic tremor: The dynamics of gas pockets trapped beneath thin permeable media. *J. Geophys. Res.* **2019**. [CrossRef]
43. Ortiz, R.; Moreno, H.; Garcia, A.; Fuentealba, G.; Astiz, M.; Pena, P.; Sanchez, N.; Tarraga, M. Villarrica Volcano (Chile): Characteristics of the volcanic tremor and forecasting of small explosions by means of materials failure method. *J. Volcanol. Geotherm. Res.* **2003**, *128*, 247–259. [CrossRef]
44. Chouet, B. Excitation of a buried magmatic pipe: A seismic source model for volcanic tremor. *J. Geophys. Res.* **1985**, *90*, 1881–1893. [CrossRef]
45. Chouet, B. Long-period volcano seismicity: Its source and use in eruption forecasting. *Nature* **1996**, *380*, 309–316. [CrossRef]
46. Hellweg, M. Physical models for the source of Lascar's harmonic tremor. *J. Volcanol. Geotherm. Res.* **2000**, *101*, 183–198. [CrossRef]
47. Johnson, J.B.; Lees, J.M. Plugs and chugs—Seismic and acoustic observations of degassing explosions at Karymsky, Russia and Sangay, Ecuador. *J. Volcanol. Geotherm. Res.* **2000**, *101*, 67–82. [CrossRef]
48. Lane, S.J.; Chouet, B.A.; Phillips, J.C.; Dawson, P.; Ryan, G.A.; Hurst, E. Experimental observations of pressure oscillations and flow regimes in an analogue volcanic system. *J. Geophys. Res.* **2001**, *106*, 6461–6476. [CrossRef]
49. Balmforth, N.J.; Craster, R.V.; Rust, A.C. Instability in flow through elastic conduits and volcanic tremor. *J. Fluid Mech.* **2005**, *527*, 353–377. [CrossRef]
50. Fujita, E.; Araki, K.; Nagano, K. Volcanic tremor induced by gas-liquid two-phase flow: Implications of density wave oscillation. *J. Geophys. Res.* **2011**, *116*, B09201. [CrossRef]
51. Jellinek, A.M.; Bercovici, D. Seismic tremors and magma wagging during explosive volcanism. *Nature* **2011**, *470*, 522–526. [CrossRef]

52. Bercovici, D.; Jellinek, A.M.; Michaut, C.; Roman, D.C.; Morse, R. Volcanic tremors and magma wagging: Gas flux interactions and forcing mechanism. *Geophys. J. Int.* **2013**, *195*, 1001–1022. [CrossRef]
53. Lipovsky, B.P.; Dunham, E.M. Vibrational modes of hydraulic fractures: Inference of fracture geometry from resonant frequencies and attenuation. *J. Geophys. Res. Solid Earth* **2015**, *120*, 1080–1107. [CrossRef]
54. Montegrossi, G.; Farina, A.; Fusi, L.; de Biase, A. Mathematical model for volcanic harmonic tremors. *Sci. Rep.* **2019**, *9*, 14417. [CrossRef] [PubMed]
55. Neuberg, J.; Tuffen, H.; Collier, L.; Green, D.; Powell, T.W.; Dingwell, D. The trigger mechanism of low-frequency earthquakes on Montserrat. *J. Volcanol. Geotherm. Res.* **2006**, *153*, 37–50. [CrossRef]
56. Chouet, B. Resonance of a fluid-driven crack: Radiation properties and implications for the source of long-period events and harmonic tremor. *J. Geophys. Res.* **1988**, *93*, 4375–4400. [CrossRef]
57. Kumagai, H.; Chouet, B. Acoustic properties of a crack containing magmatic or hydrothermal fluids. *J. Geophys. Res.* **2000**, *105*, 25493–25512. [CrossRef]
58. Neuberg, J.; O'Gorman, C. A Model of the Seismic Wavefield in Gas-Charged Magma: Application to Soufrière Hills Volcano, Montserrat. In *The Eruption of Soufrière Hills Volcano, Montserrat, from 1995 to 1999*; Druitt, T.H., Kokelaar, B.P., Eds.; Geological Society of London: London, UK, 2002; Volume 21, pp. 603–609.
59. Manga, M. Waves of bubbles in basaltic magmas and lavas. *J. Geophys. Res.* **1996**, *101*, 17457–17466. [CrossRef]
60. Michaut, C.; Ricard, Y.; Bercovici, D.; Sparks, R.S.J. Eruption cyclicity at silicic volcanoes potentially caused by magmatic gas waves. *Nat. Geosci.* **2013**, *6*, 856–860. [CrossRef]
61. Spina, L.; Cimarelli, C.; Scheu, B.; Di Genova, D.; Dingwell, D.B. On the slow decompressive response of volatile- and crystal- bearing magmas: An analogue experimental investigation. *Earth Planet. Sci. Lett.* **2016**, *433*, 44–53. [CrossRef]
62. Jousset, P.; Neuberg, J.; Sturton, S. Modelling the time-dependent frequency content of low-frequency volcanic earthquakes. *J. Volcanol. Geotherm. Res.* **2003**, *128*, 201–223. [CrossRef]